Ocean Data Assimilation: A Coastal Application

Xiaodong Hong, James A. Cummings, Paul J. Martin and James D. Doyle

Abstract The Navy Coupled Ocean Data Assimilation (NCODA) system is applied to a period during the Autonomous Ocean Sampling Network II (AOSN II) field campaign conducted in the Monterey Bay area in August 2003. The multivariate analysis of NCODA is cycled with the Navy Coastal Ocean Model (NCOM) in a sequential, incremental, update cycle. In addition to the operational data obtained from the Global Ocean Data Assimilation Experiment (GODAE) server, which included satellite observations of sea-surface temperature (SST) and sea-surface height and insitu surface and sub-surface observations of temperature and salinity, high-density data from aircraft SST observations and high-frequency data from buoys used for the AOSN II field experiment are also assimilated. The results from data assimilative and non-assimilative runs are compared with and verified against observations. Bias and root-mean-square errors of temperature indicate that forecast skill from the data assimilative run exceeds errors from the persistence and the non-assimilative runs. The seasonal thermocline is better represented and the warm bias for both upwelling and relaxation periods is significant reduced.

1 Introduction

Coastal ocean forecast uncertainty stems from uncertainty in the ocean model physics and numerics, air-sea fluxes, lateral boundary conditions, initial conditions, and bathymetry. To reduce the uncertainty of an ocean forecast, an ocean data assimilation system is needed to better estimate the ocean state and model parameters by combining observed ocean data with the governing physics and dynamics of the ocean model. There are a number of ocean data assimilation schemes based on different theories and methods to optimally or sub-optimally provide state estimation in space and time. Compared to the use of data assimilation in meteorology, ocean data assimilation has a much shorter history. Blue water models are very well constrained at the surface using altimeter sea surface height (SSH). However, it is difficult to constrain models in coastal areas due to the inherent short time/space scales and

X. Hong (✉)

Marine Meteorology Division, Naval Research Laboratory, Monterey, CA 93943, USA

lack of high frequency ocean observations (other than moorings). In recent years, unprecedented in situ observational tools, such as sophisticated autonomous robotic vehicles, aircraft, CODAR (Coastal Ocean Dynamics Applications Radar), drifters, etc., have been increasingly used to collect data qualitatively and quantitatively in various coastal ocean field experiments. These data provide opportunities for testing and validating data assimilative forecast schemes. These evaluations, in turn, can help to identify model deficiencies and lead to improved forecast models.

The ocean data assimilation system used here is NCODA (Cummings 2005). NCODA is currently being applied in real time at Fleet Numerical Meteorology and Oceanography Center (FNMOC) and at the Naval Oceanographic Office (NAV-OCEANO). It can be executed as a stand-alone analysis or cycled with an ocean forecast model in a sequential, incremental, update cycle. The ocean forecast models that have been cycled with NCODA include the Hybrid Coordinate Ocean Model (HYCOM), the Navy Coastal Ocean Model (NCOM), the parallel Ocean Prediction Ocean model (POP), and the Shallow Water Analysis Forecast System (SWAFS), which is based on the Princeton Ocean Model. In this study, the NCOM forecast model (Martin 2000) is cycled with the NCODA system.

In this application, NCOM uses initial and lateral boundary conditions from the Navy's operational global NCOM forecast system. The surface atmospheric forcing for NCOM is provided from real-time forecasts by the Navy's Coupled Ocean/Atmosphere Mesoscale Prediction System (COAMPS®)[1] (Hodur 1997).

The execution of NCODA cycled with NCOM during a coastal field campaign is performed and evaluated in this study. The field campaign is the Autonomous Ocean Sampling Network (AOSN) II conducted in Monterey Bay during August 2003. The objective of AOSN II is to develop an adaptive, coupled, observational/modeling prediction system capable of providing an accurate 3- to 5- day forecast of marine-biology events. The regional circulation near the Monterey Bay can be described in two distinct hydrographic states: upwelling state and relaxed state. The upwelling is driven by the prevailing north/northwesterly wind (i.e., directed towards the south/southeast). Two upwelling centers are formed at headlands to the north of the bay at Point Ano Nuevo and south at Point Sur. During the upwelling periods, there is a cyclonic circulation (or eddy, Tseng and Breaker 2007) in the bay and an anticyclonic California Current meander, also sometimes referred to as the Monterey Bay Eddy (Ramp et al. 2005), offshore of the bay. When the wind relaxes, the upwelling reduces, and the offshore eddy moves into the bay and interacts with the flow over the shelf.

The mesoscale circulations in the vicinity of Monterey Bay are highly complex and variable. It is difficult to model these features correctly due to the errors resulted from model dynamics, model resolution, bathymetry, atmospheric forcing and lateral boundary conditions. Fortunately, we have a data assimilation system in place so that data collected from the field experiment can be used for data assimilative simulation to compensate the drawback in numerical simulation. The purposes of this work are to use observational data obtained from the AOSN II field campaign to

---

[1] COAMPS®, COAMPS is a registered trademark of the Naval Research Laboratory

perform data assimilative simulation of upwelling/relaxation processes in the vicinity of Monterey Bay and to assess the skill of the data assimilative simulation.

Section 2 briefly describes the components of the ocean data-assimilation system. The configuration of the data-assimilation system is described in Sect. 3. Information about the observations that are assimilated is provided in Sect. 4. Results from the assimilative simulation are discussed and compared with the observation from the AOSN II field experiment in Sect. 5. Verification and evaluation of the ocean data assimilation system are shown in Sect. 6. Summary and conclusions are presented in Sect. 7.

2 Brief Description of Each Component

2.1 NCODA

NCODA is a fully three-dimensional, multivariate, optimum-interpolation (MVOI) (Daley 1991) ocean-data assimilation system that produces simultaneous analyses of temperature, salinity, geopotential (dynamic height), and vector velocity. A complete description of NCODA can be found in Cummings (2005). The formulation is as:

$$\mathbf{x_a} = \mathbf{x_b} + \mathbf{P_b}\mathbf{H}^T(\mathbf{H}\mathbf{P_b}\mathbf{H}^T + \mathbf{R})^{-1}\{\mathbf{y} - \mathbf{H}(\mathbf{x_b})\} \tag{1}$$

where $\mathbf{x_a}$ is the analysis vector, $\mathbf{x_b}$ is the background vector, $\mathbf{P_b}$ is the background-error covariance matrix, $\mathbf{H}$ is the forward operator, $\mathbf{R}$ is the observation error covariance matrix, and $\mathbf{y}$ is the observation vector.

The observation vector $\mathbf{y}$ contains all of the synoptic temperature, salinity, and velocity observations that are within the geographic and time domains of the forecast model grid and update cycle. The forward operator $\mathbf{H}$ is a spatial interpolation of the forecast model grid to the observation locations performed in three dimensions. Thus, $\mathbf{H}\mathbf{P_b}\mathbf{H}^T$ is approximated directly by the background-error covariance between the observation locations, and $\mathbf{P_b}\mathbf{H}^T$ directly by the error covariance between the observation and grid locations. The quantity $\{\mathbf{y} - \mathbf{H}(\mathbf{x_b})\}$ is referred to as the innovation vector, $\{\mathbf{y} - \mathbf{H}(\mathbf{x_a})\}$ is the residual vector, and $\mathbf{x_a} - \mathbf{x_b}$ is the increment (or correction) vector.

The background-error covariances are separated into a background-error variance and a correlation. The correlation is further separated into a horizontal and a vertical component. NCODA uses flow-dependence covariances in the analysis by scaling the horizontal and vertical correlations with a correlation computed from the geopotential height difference between two locations. The horizontal correlation length-scales are specified as the first baroclinic Rossby radius of deformation computed from the historical profile archive (Chelton et al. 1998). The vertical correlation length-scales can be either constant (used in this study), monotonically increasing or decreasing with depth, or varying with background density vertical gradients.

All analysis variables use the same background-error second-order autoregressive correlation model for calculating the horizontal correlations.

Background-error variances vary with location, depth, and analysis variable. They are related to the analysis increments and expectations based on the age of the data on the grid. The background-error variances are allowed to increase with time in the long-term absence of observations until the errors asymptote at the limit of the expected variance, specified as either climate variability or model error. The climate variability is specified in this study due to the lack of availability of model error from the global NCOM system.

The observation errors and the background errors are assumed to be uncorrelated, and errors associated with observations made at different locations and at different times are also assumed to be uncorrelated. Observation errors are computed as the sum of a measurement error and a representation error. Most measurement-error variances are specified as input parameters based on fairly well-known ocean observing errors. One exception is for the geopotential observations. Geopotential errors are computed from the observation errors of the potential temperature and salinity, using the partial derivatives of the equation of state. Representation errors are a function of the resolutions of the model and of the observing network.

Altimeter sea surface height (SSH) is assimilated from synthetic temperature profiles computed using the Modular Ocean Data Assimilation System (MODAS) database. MODAS provides the time-averaged co-variability of SSH and temperature at depth at a fixed location (Fox et al. 2002).

All ocean observations are subject to data quality-control (QC) procedures prior to assimilation. The need for quality control is fundamental in the analysis system; erroneous data can cause an incorrect analysis, while rejecting extreme data can miss important events. The primary purpose of the QC system is to identify observations that are obviously in error, as well as the more difficult process of identifying measurements that fall within valid and reasonable ranges, but are erroneous. A secondary use of the QC system is the creation and maintenance of an analysis-forecast increment database for use in the a posteriori computation of the optimum interpolation statistical parameters. A detailed description of the real-time QC system can be found in Cummings (2006).

2.2 NCOM

NCOM is a three-dimensional, primitive equation, free-surface model using the hydrostatic, Boussinesq, and incompressible approximations. Details of the model description can be found in Martin (2000). NCOM is designed to offer the user a range of numerical choices in terms of parameterizations, numerical differencing, and vertical grid structure. NCOM uses a hybrid vertical coordinate system, which allows for the use of all sigma-layers, or all z-levels, or a combination of the sigma-layers for the upper ocean and z-levels below. The model equations are solved on a staggered, Arakawa C-grid. Temporal differencing is leap-frog with an Asselin filter to suppress time splitting. Spatial averages and finite differences are mainly second

order with an option for higher-order formulations for advection. The propagation of surface waves and vertical diffusion is treated implicitly. The Mellor-Yamada Level 2.5 turbulence scheme is used for vertical mixing. NCOM forcing includes surface air-sea fluxes, lateral open boundary conditions, tides, and river and runoff discharges.

NCOM has been applied to many locations, including the Adriatic Sea (Pullen et al. 2003) and Monterey Bay (Shulman et al. 2007) to study fine-scale oceanic features under atmospheric forcing with different resolution, and the Gulf of Lion to study the effects of time variation of the surface buoyancy flux on the formation of deep-water convection during the winter season (Hong et al. 2008). A recent application is the development of NCOM ensemble forecasting (Hong and Bishop 2005) using the ensemble transform technique (Bishop and Toth 1999) and adaptive sampling for coastal observations (Hong and Bishop 2006) using the ensemble transform Kalmar filter method (Bishop et al. 2001).

2.3 Atmospheric forcing

The atmospheric forcing for NCOM consists of the surface air pressure, wind stress, heat flux, and effective surface salt flux for the momentum, temperature, and salinity equations. For this study, these are provided from COAMPS atmospheric forecasts in hourly frequency. COAMPS is a fully compressible, nonhydrostatic, primitive equation model based on a staggered, C grid and solved using a time-splitting technique with a semi-implicit formulation for the vertical acoustic modes (Hodur 1997; Hodur et al. 2002; Doyle et al. 2008). A Robert time filter is used to damp the computational mode. All derivatives are computed to second-order accuracy and options are provided for forth-order accurate horizontal advection and diffusion. COAMPS uses parameterization schemes for subgrid-scale convection, shortwave and longwave radiation processes, and mixed-phase cloud microphysics. A three-dimensional, multivariate, optimum-interpolation (MVOI), analysis technique is used to map the observations to the model grid and generate the initial conditions for the forecast model for each data assimilation cycle. Quality-controlled data used in the analysis are radiosonde, aircraft, satellite, and surface observations. Additional information about the atmospheric model set-up and forecast skill during AOSN II is discussed in Doyle et al. (2008).

To allow some interactive feedback from the ocean model, the surface latent and sensible heat fluxes for NCOM are computed from the COAMPS wind speed and air temperature and humidity and the NCOM-predicted sea-surface temperature (SST) using the drag coefficient from the standard bulk formulas of Kondo (1975) (Martin and Hodur 2003). The surface salt flux for NCOM is calculated from the computed latent heat flux and the COAMPS precipitation. The extinction of solar radiation in seawater as classified by Jerlov (1976) according to turbidity was used in the model with six optical types to define the subsurface penetration of the COAMPS solar radiation.

3 Configuration

The computational domain, grid projection, and horizontal resolution for NCODA and NCOM are the same to minimize the errors from the horizontal interpolation of fields between the two systems. The ocean-model domain covers both the Monterey and San Francisco Bay areas (Fig. 1a) and is within the innermost grid of COAMPS (Fig. 1b) (e.g. Doyle et al. 2008). The grid projection is Lambert conformal with a horizontal spacing of 3 km. In the vertical, NCOM uses a total of 40 layers with 15 sigma-layers in the upper ocean and 25 z-levels in the deeper water. The vertical resolution ranges from 1 to 500 m. NCODA uses 30 standard depth levels with a maximum depth of 3000 m. The horizontal grid size for both NCODA and NCOM is 96×168. The $1/8°$ global NCOM real-time nowcast for 1 August 2003 is used to start NCOM before data assimilation cycle takes place. The lateral boundary conditions for the regional NCOM are also supplied from the global NCOM and updated at a 3 h frequency. The lateral boundary conditions are important for providing large-scale forcing, such as California current, through the open boundaries of the regional model.

The COAMPS forecasts are produced twice daily out to 72 h using a 12 h, incremental, data-assimilation cycle on a quadruple-nested grid system with horizontal resolutions of 81, 27, 9, and 3 km (Fig. 1b). The innermost grid has dimensions $199 \times 199 \times 30$. The COAMPS surface fields from the innermost nest with high-resolution are output on an hourly basis to force NCOM. The high-resolution COAMPS surface winds provide good representation of the narrow
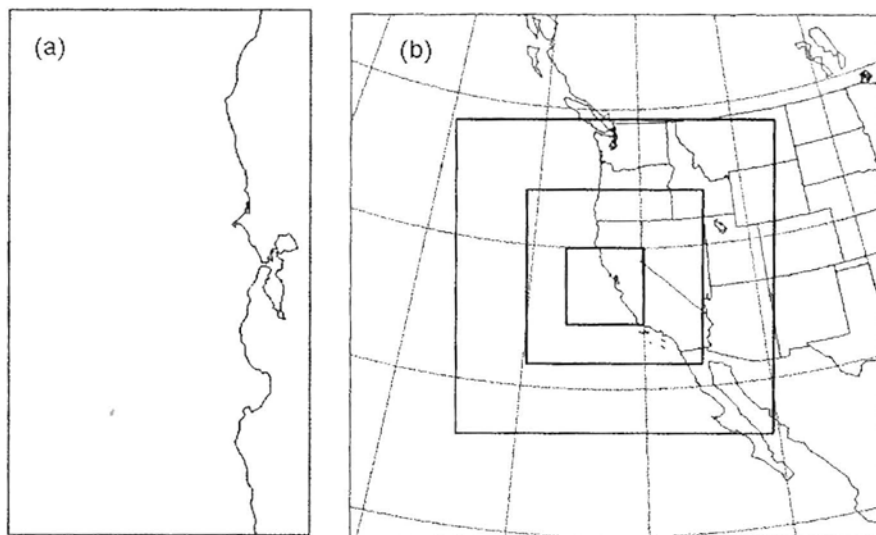

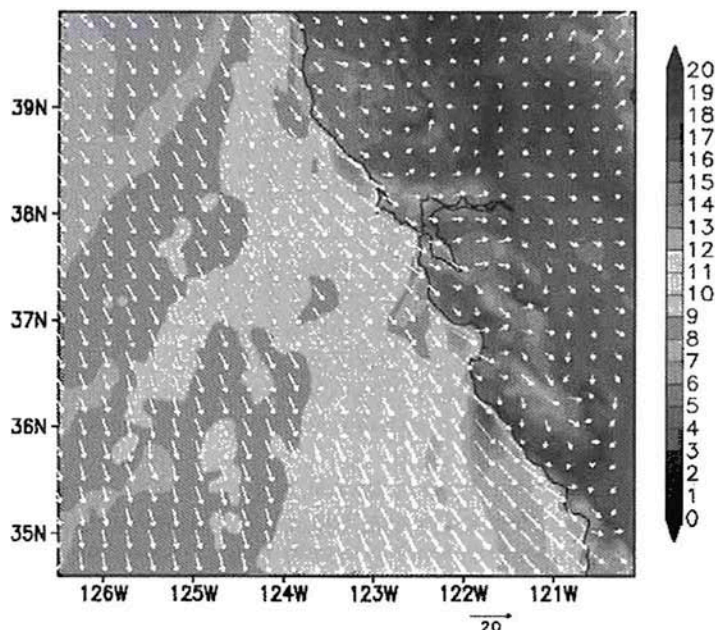**Fig. 1** (a) The NCODA and NCOM domain; (b) The COAMPS nested domain

Fig. 2 COAMPS 10 m wind speed (ms^{-1}) valid at 23Z August 11, 2003 from the innermost nest with horizontal resolution of 3 km

bands (about 10 by 50 km) of strong wind stress and wind stress curl (Fig. 2), which are very important to the generation of upwelling along the California coast (Pickett and Paduan 2003). These narrow bands are parallel to the coast and adjacent to major California coastal promontories, causing upwelling through Ekman transport. Observations of SST from satellites have shown that cold-water plumes off northern California are frequently anchored to coastal topography (Kelly 1985).

The assimilative system is performed in a sequential incremental update cycle with an update interval of 24 h. NCODA uses NCOM 24 h forecast fields of temperature, salinity and velocity as first guess fields and assimilates all available observations within the update-cycle time window so that it allows the use of background information closest to the observation time. The analysis fields are used to initialize the NCOM forecast at each analysis time.

In order to quantify the improvement of the forecast by data assimilation, two experiments are conducted for entire month of August 2003. The first experiment is run with data assimilation and produces 72 h forecast at each analysis update time based on a 24 h update cycle. The second experiment is a case with NCOM being integrated forward from August 1 to 31, 2003 without any data assimilation. The first experiment is referred to as the "assimilative run", while the second one is referred to as the "non-assimilative run".

4 Observations

Observations used in the ocean analysis include all sources of operational ocean observations. They contain remotely-sensed SST from AVHRR GAC infrared satellite, sea surface height from satellite altimeters, in situ surface and sub-surface observations of temperature and salinity from a variety of sources, such as ships, buoys, expendable bathythermographs, and conductivity-temperature-depth sensors. A description of the operational data sources can be found in Table 1 in Cummings (2005). We display here the types, paths, locations of observation data for one particular analysis time as an example in Fig. 3. The number of observations for each analysis cycle is also provided in the validation section. These data have been quality controlled and archived in the Global Ocean Data Assimilation Experiment (GODAE) server hosted by the Fleet Numerical Meteorology and Oceanography Center (FNMOC).

In addition to the operational observations, aircraft SST data collected during the AOSN II field campaign in August 2003 by the Naval Postgraduate School (NPS) (Ramp 2003) and continuous time series of data from the MBARI buoys m1 (Chavez 2003a) and m2 (Chavez 2003b) are also assimilated. The airborne measurements were made using a twin-engine, eight-seat, Piper Navajo owned and operated by Gibbs Flite Center (Ramp et al. 2005). The plane typically flew below the
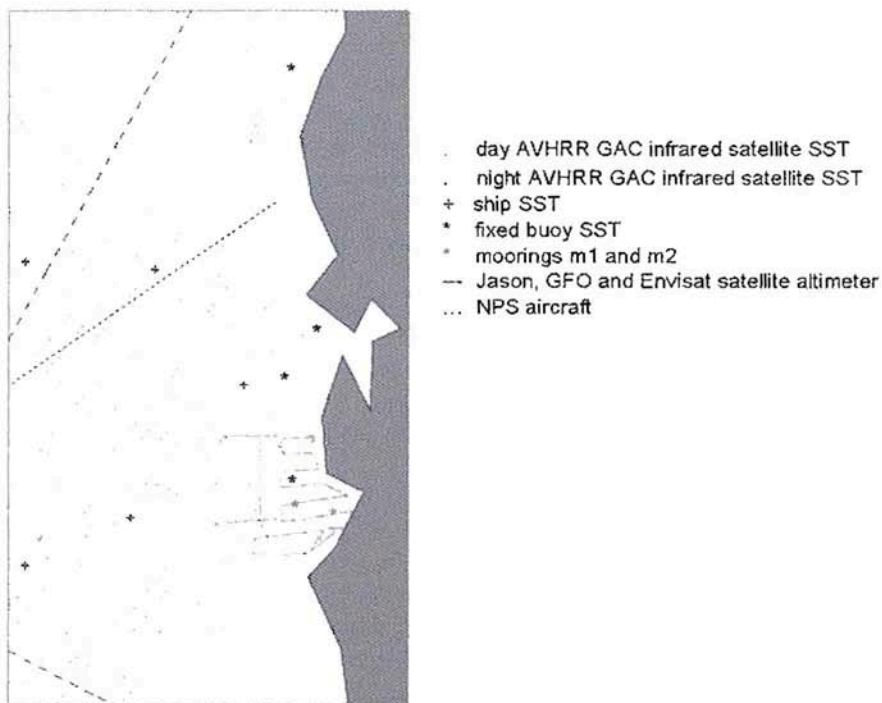

.   day AVHRR GAC infrared satellite SST
.   night AVHRR GAC infrared satellite SST
+   ship SST
*   fixed buoy SST
°   moorings m1 and m2
--   Jason, GFO and Envisat satellite altimeter
...   NPS aircraft

Fig. 3 Observation types and locations used in the assimilation for 13 August 2003

quasi-permanent, summertime, stratus deck and provided a spatial context for the relative sparse in situ observations. The airborne data were collected at 1 Hz resolution and included pressure, temperature, dew point, relative humidity, and SST. A Heitronics KT-19 infrared radiation pyrometer was used to measure SST with 0.1°C precision and 0.5°C absolute accuracy. Sample aircraft paths for 13 August 2003 are shown using red-dashed lines in Fig. 3. There are a total of 12 daily flights during the August 2003 AOSN II field experiment, from which the measured SSTs are quality controlled and assimilated in this study.

The m1 and m2 MBARI buoys are located at (36.75°N, 122.03°W) and (36.7°N, 122.39°W) (green-asterisks in Fig. 3), respectively. Both of the moorings provide data in real time from the surface to 300 m at 10-min intervals. These high-frequency temperature and salinity profiles from m1 and m2 are quality controlled and assimilated in this study.

5 Comparisons of Assimilative Results with Observations

The upwelling/relaxation features during the AOSN II experiment in August 2003 are explored using the results from the data assimilative simulation. At this time, the winds over Monterey Bay can be described as periods that are upwelling favorable with north/northwesterly or upwelling unfavorable with south/southwesterly (see Doyle et al. 2008). The corresponding wind stresses are shown in Fig. 4a.
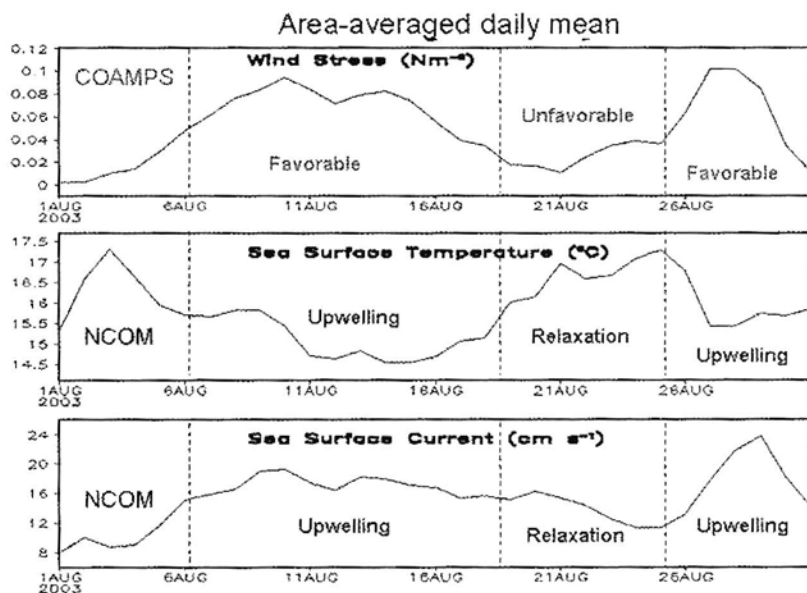

Fig. 4 Area-averaged daily mean for surface (**a**) wind stress, (**b**) temperature, and (**c**) current. The area is within 36.2–37.2°N and 123–121.6°W

As a result, the regional circulation corresponds to an upwelling state and a relaxation state. The winds in early August are not favorable for upwelling. From August 7 to 19, the prevailing north/northwesterly winds (i.e., directed towards the south/southeast) are re-established and induce upwelling. Warmer surface waters are forced offshore, allowing cold waters to rise to the surface near the coast. The surface temperature averaged over the Monterey Bay area is significantly reduced and the averaged surface current speed increases (Fig. 4b, c). From August 20 to 24, the winds are light with a south or southwest direction, resulting in relaxation conditions. During this period, upwelling along the coast diminished and the warm offshore water moved shoreward. The area-averaged surface temperature increases and surface current speed decreases. During the latter portion of August, there is a short period of upwelling when the northwesterly wind is onset again around the bay.

Significant diurnal fluctuations in upwelling occur during the data assimilative simulation associated with diurnal fluctuations in the surface atmospheric conditions (see Fig. 5). These resemble a classic sea-breeze circulation pattern forced by large surface heating differences between the coastal marine atmosphere and the Central Valley (Banta et al. 1993). In Fig. 5, at the north upwelling center (Point Ano Neuvo) the simulated SST decreases and the sea-surface salinity (SSS) increases during the upwelling period and vice versa during the relaxation period. The diurnal fluctuations for wind stress, SST, and SSS are superimposed on the longer-period changes
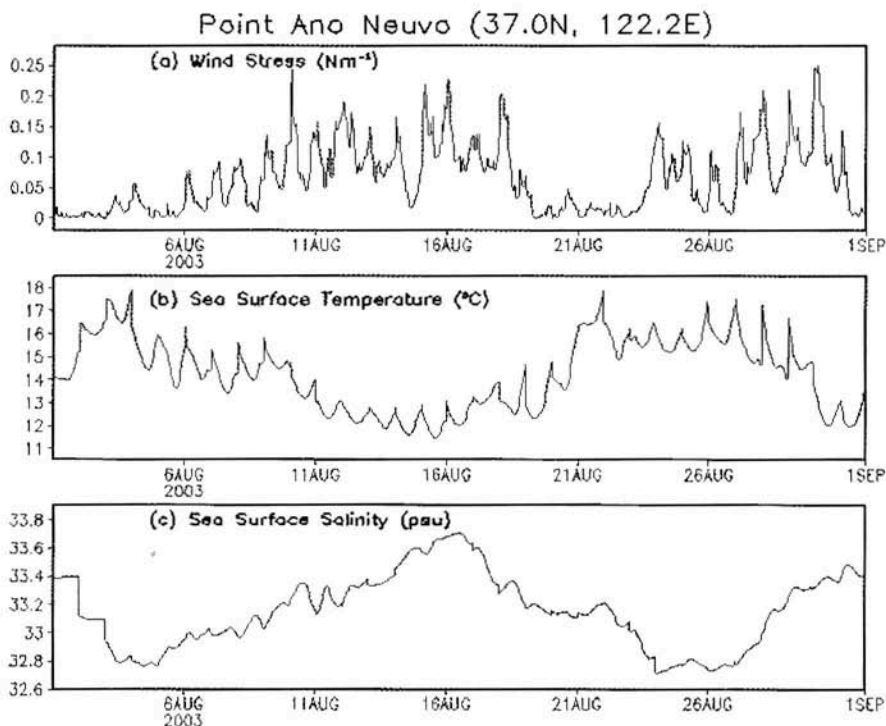

Fig. 5 Hourly (a) surface wind stress, (b) temperature, and (c) salinity at Point Ano Neuvo

associated with the upwelling and relaxation events. The peak upwelling takes place
on August 16 as indicated by the lowest surface temperature and salinity.

5.1 Upwelling Period

Two upwelling centers develop off Point Ano Nuevo and Point Sur during the up-
welling period from 7 to 19 August. Figure 6a shows the SST forecast for 18 h (valid,
at 18Z August 15, 2003) using the assimilation of observed data as shown in Fig. 3.
The assimilation realistically depicts the signature of the upwelling since it has been
proceeding for several days. The coldest upwelled water in the upwelling center off
Point Ano Nuevo reaches 11.5 °C at this time. Large horizontal SST gradients oc-
cur between the upwelled cold water and the offshore warm water. A cold tongue
of upwelled water off Point Ano Nuevo is advected southward across the mouth
of Monterey Bay. The plume of upwelled cold water extends southward and joins
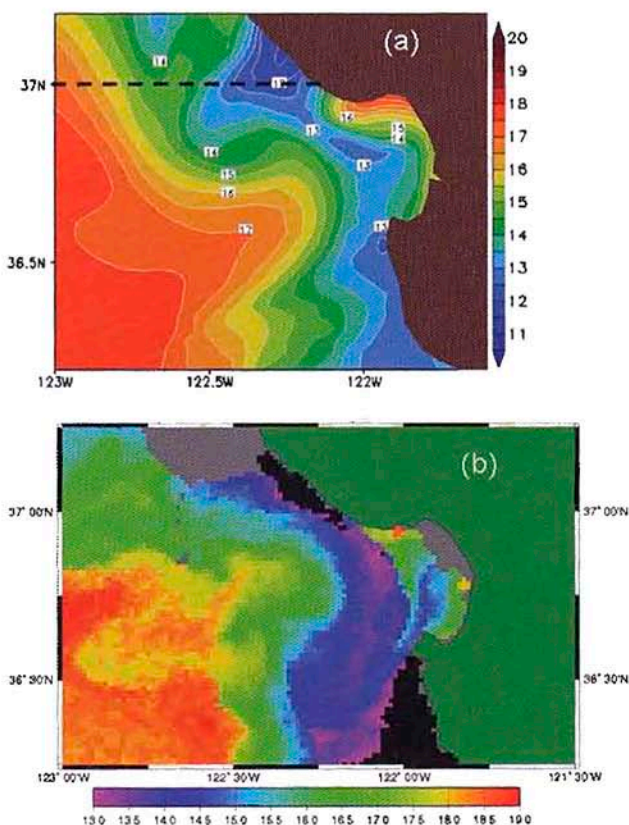with the upwelled cold water from Point Sur, resulting in a large, cold-water region

Fig. 6 (a) SST from 18 h forecast valid at 18Z August 15, 2003. (b) NOAA POES AVHRR HRPT
SST at 1858Z August 15, 2003 (NOAA POES AVHRR, Courtesy NWS and NOAA Coastwatch)

located just off the coast. Upwelled cold water also may have advected seaward as suggested in a previous observational study (Rosenfeld et al. 1994).

The NCOM SST assimilative forecasts are compared with the Coastwatch SST produced from the AVHRR High Resolution Picture Transmission (HRPT) data and broadcasted continuously by the Polar Orbiting Environmental Satellites (POES) by NOAA's National Environmental Satellite, Data, and Information Service (NES-DIS) (see Fig. 6b). The HRPT data have a resolution of 1.1 km and are mapped to almost full resolution in the production of the CoastWatch AVHRR visible, infrared, and SST images. The AVHRR HRPT SST data are not used in the data assimilation experiments, but the 4-km global area coverage (GAC) SST retrievals from several NOAA satellites are assimilated. The basic observed features are captured by the NCOM forecast as displayed in Fig. 6a for the 18 h SST forecast valid at the satellite observational time (Fig. 6b). These include (1) strong upwelling off Point Ano Neuvo and Point Sur, (2) upwelled water advected southward across the mouth of Monterey Bay that joined with cold water from Point Sur, and (3) warmer offshore water advected toward the mouth of Monterey Bay.

Figure 7 shows a vertical cross section of forecast temperature at 18 h along 37.05 °N at 18Z August 15, 2003. The isopleths of temperature are sloped upward towards the coast, indicating that the upper-layer warm water is pushed offshore and deep cold water is brought to the surface by Ekman transport and
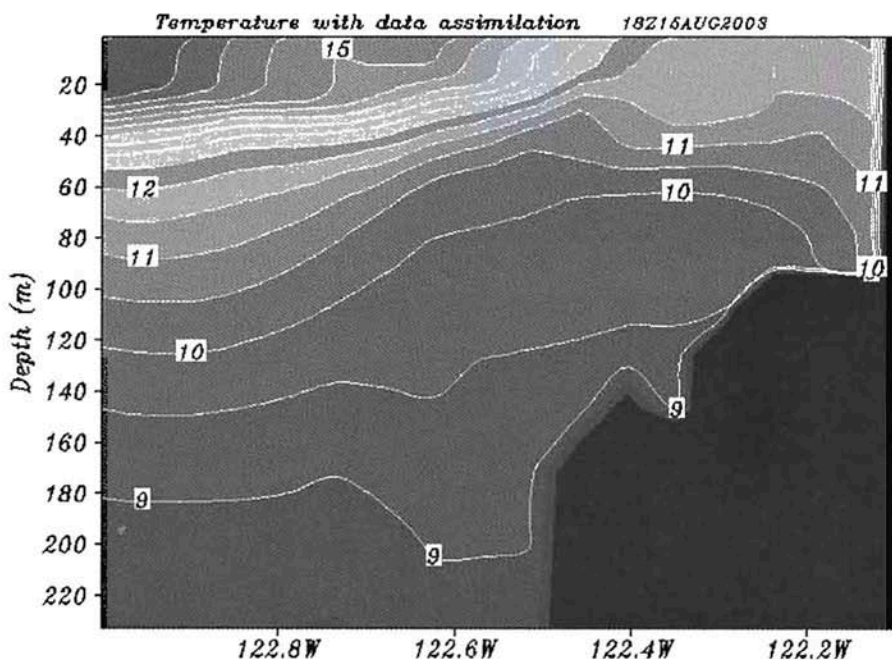

Fig. 7 Vertical cross section of temperature on 18 Z August 15, 2003 along 37.0°N as a dashed-line shown in Fig. 6
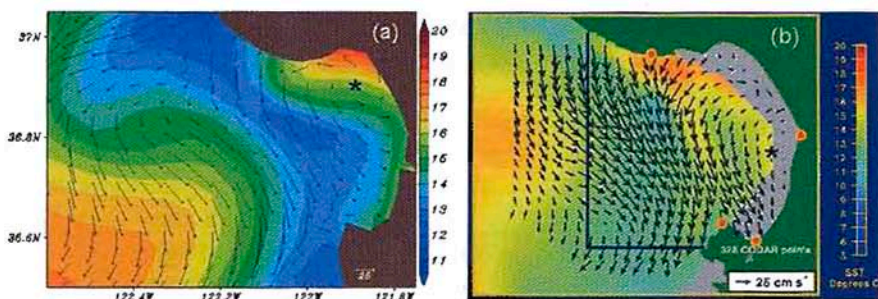
Fig. 8 25 h mean from 5Z August 15 to 6Z August 16 2003 for (a) NCOM surface temperature and current, (b) HF radar surface current with AVHRR-derived SST (Paduan and Lipphardt 2003). The approximated locations of cyclonic centers are marked as "*"

pumping (Pickett and Paduan 2003). An upwelling front exists between the up-welled and offshore water with a characteristic gradient of 5°C per 100 km across the front.

The NCOM forecast surface current was also compared with the NPS mean HF radar surface currents (Paduan and Lipphardt 2003). The HF radar surface current data were not used in the data assimilation. The comparison of surface current was made for a 25 h mean from 5Z August 15 to 6Z August 16, 2003 during the peak of the upwelling event (Fig. 8). The forecast model shows that cold, upwelled water from Point Ano Nuevo was advected across and into the mouth of Monterey Bay and joined with cold water off Point Sur south of Monterey Bay (Fig. 8a). Both the model and the HF radar show a cyclonic circulation in the bay. However, the size of the cyclonic circulation is smaller in the model and its location is confined within the northern part of the bay. This may be caused by the stronger, southeastward current in the model simulation that advected cold water into the southern part of Monterey Bay. The model results show the warm water offshore in the area of anti-cyclonic circulation to be advected further to the south and closer to the bay. The larger area of cold water in the southern part of Monterey Bay and the stronger warm offshore meander could be due to insufficient model resolutions in both atmospheric and ocean models.

5.2 Relaxation Period

An anti-cyclonic meander within the California current moves coastward and cold upwelled water is replaced by warm offshore water during the relaxation period. Figure 9a indicates that warm water occupied the most area with temperatures above 16°C at the surface. Cold water still exists in both upwelling centers; however, the areal extent is considerably reduced as can be seen from the model forecast (Fig. 9a) and from the AVHRR SSTs (Fig. 9b) with the coldest water temperature not less than 14°C. Since there is much less data available for this period as will be seen
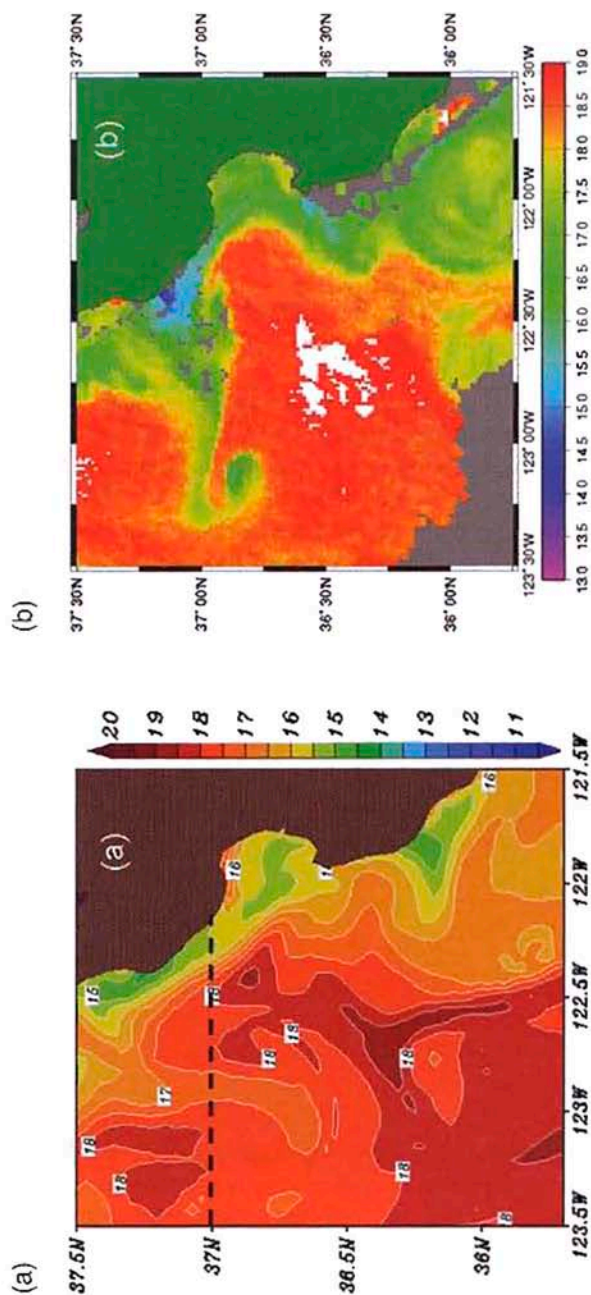
Fig. 9 (a) NCOM SST from 18 h forecast valid at 18Z August 24, 2003. (b) NOAA POES AVHRR HRPT SST at 1856Z August 24, 2003 (NOAA POES AVHRR, Courtesy NWS and NOAA Coastwatch)

in the validation section, the errors in the model representation of the relaxation episode is most likely due to errors in the atmospheric forcing.

The isopleths of temperature slope downward towards the coast during the relaxation stage (Fig. 10), indicating that offshore warm water is advected to the nearshore. Downwelling forced the upper-layer water downward following the slope of the topography. The upwelling front is located near the coast. Warm water recapped the surface layer in the original upwelling area. There still exist smaller temperature gradients across the front with about a 2.0°C difference.

The 25 h mean NCOM forecast from 5Z August 25 to 6Z August 26, 2003 for a relaxed state is compared to the 25 h mean HF radar observation for the same time period (Fig. 11). Both the model and the data show slightly colder water in the southern part of the bay, a cyclonic circulation inside the bay, and an anti-cyclonic circulation outside the bay. The size and strength of these two circulations are similar in the HF radar analysis. However, the forecast model shows a smaller current speed for the cyclonic circulation inside the bay than for the anti-cyclonic circulation outside the bay. This again could be a result of the coarse horizontal resolution used in the NCOM. The high frequency HF radar can provide significant detail of the surface current in Monterey Bay and allow mesoscale features, like coastal eddies to be resolved with much more accuracy than an array of current meters. In the future, these current data will be used in the assimilation.
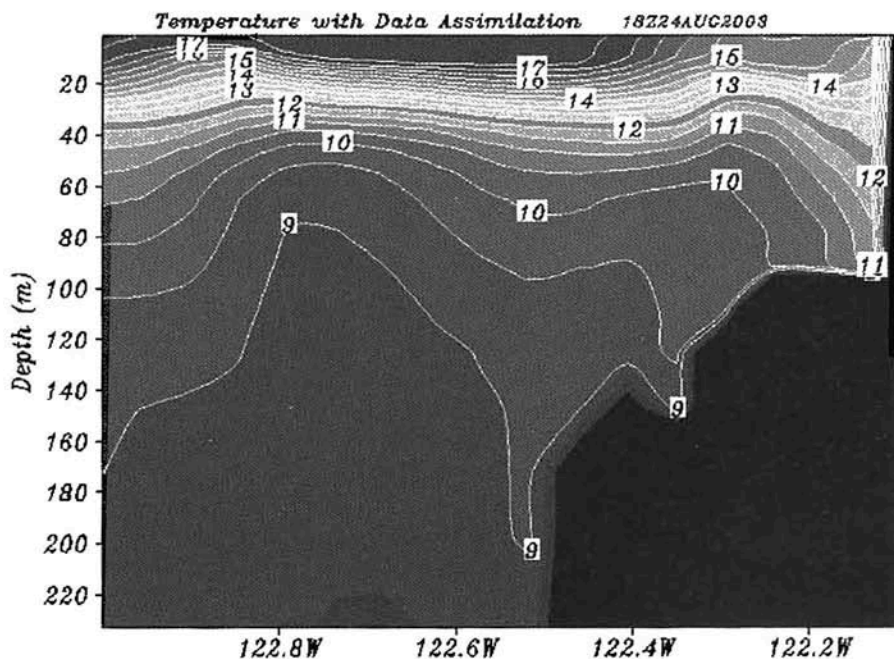

Fig. 10 Vertical cross section of temperature along 37.0°N on 18 Z August 15, 2003 as a dashed-line shown in Fig. 9
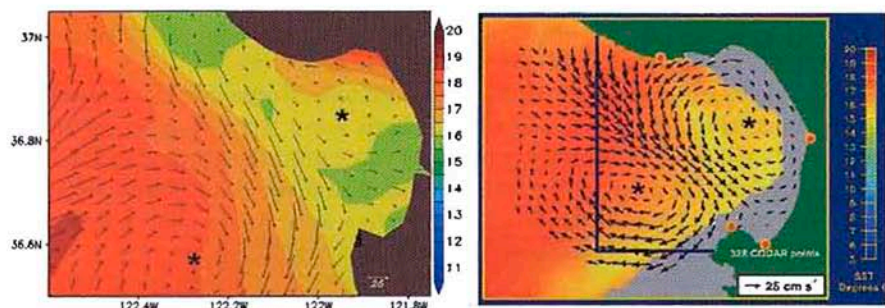
Fig. 11 25 h mean from 5Z August 25 to 6Z August 26, 2003 for (a) NCOM surface temperature and current, (b) HF radar surface current with AVHRR derived SST (Paduan and Lipphardt 2003) The approximated locations of cyclonic centers are marked as "*"

6 Validation

The innovations and residuals for all assimilated observations are saved at the end of each update cycle so that assessment of the impact of the assimilation on the skill of the forecast can be made and the fit of the analysis to specific observations or observing systems can be evaluated.

The innovation and residual root-mean-square error (RMSE) and bias for any analysis or forecast variables are calculated as:

$$RMSE = \sqrt{\frac{1}{N}\{H(x) - y\}^2} \tag{2}$$

$$bias = \frac{1}{N}\{H(x) - y\} \tag{3}$$

where N is the number of observation data used in the analysis and x represents any analysis or forecast variable.

Time series of innovation and residual bias and RMSE for SST and temperature averaged over depth are shown in Fig. 12. Figure 12a and 12b show SST RMS and mean bias errors decreasing with time during the first 3–5 days of the assimilation. After this time the SST innovation errors tend to stabilize suggesting that the model is accepting and retaining information from assimilation of the data. The mean SST innovation RMS error for the entire month is 0.73°C, with a mean bias error of −0.11°C. The analysis consistently reduces forecast errors throughout the assimilation time period. Mean SST residual RMS and bias errors are 0.28°C and −0.01°C, respectively. Similar patterns of reduction in RMS and mean bias errors from the forecast to the analysis are seen for temperature at depth (Fig. 12c, d), although relatively few subsurface observations were available. Nevertheless, forecast RMSE errors at depth are reduced from 0.95 to 0.35°C and forecast mean bias errors are reduced from 0.07 to −0.01°C by the analysis. SST forecast errors tend to be large following periods when few observational data are available for the assimilation

Fig. 12 (a) RMSE and
(b) bias for SST innovation
and residual, (c) RMSE and
(d) bias for temperature
innovation and residual, and
(e) number of observation for
SST and temperature
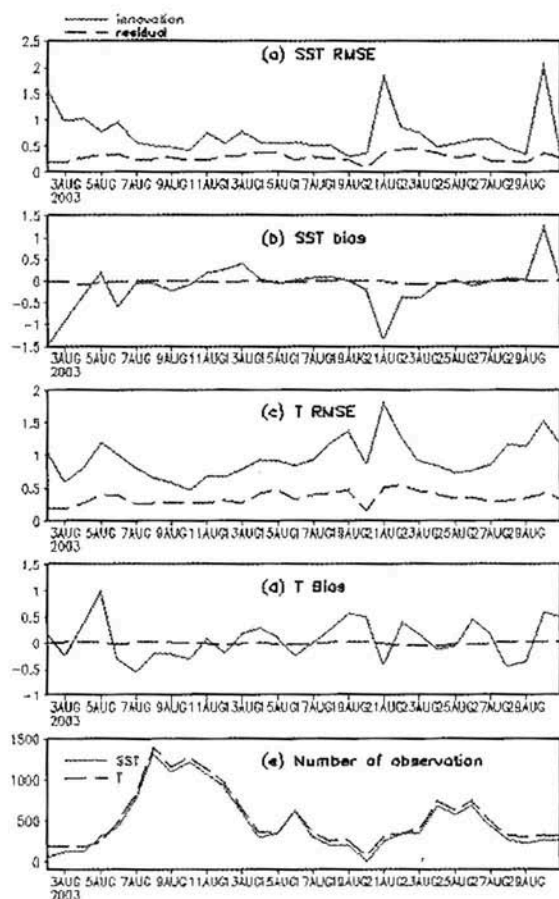
(compare forecast errors on August 22 with data counts on August 20). This suggests that the high surface variability associated with upwelling and relaxation processes in the Monterey Bay will require continuous observations in order to maintain forecast skill at 2 days. Further, the lack of forecast skill during the transition stage between upwelling and relaxation that started on August 20 may also be related to inaccuracies in the ocean model and the atmospheric forcing.

The consistent reduction in RMS error from the forecast to the assimilation throughout the assimilation time period given the changes in observation locations is an indication of a stable analysis/forecast system. This result is further indicated by the zero residual mean bias errors over all update cycles in conjunction with monthly averaged innovation bias errors that are essentially zero. A zero residual mean bias is an expected outcome from a least squares procedure such as optimum interpolation. A non-zero residual mean bias would be an indication of problems in the implementation of the analysis algorithm or in the pre-processing of the observations. A near zero innovation mean bias provides good evidence that, on average, the assimilative ocean model does not have any systematic model errors at the 24 h update cycle forecast period.

The forecast skill is evaluated by comparing the model RMSE at lead forecast times of 24, 48, and 72 h with the RMSE from persisting the previous analysis (nowcast) for the same lead time. The validation time period is from 2 to 31 August with an update assimilation cycle every 24 h, which yields 30 analyses. The forecast and persistence RMSE for SST are summarized from the domain mean values as shown in Fig. 13. The forecast RMSE from non-assimilative run is included and displayed as red solid line. The results show that model forecasts of SST are more skillful than persistence when data assimilation is performed. The SST forecast improvement over persistence is more significant as the forecast lead time increases, indicating that the persistence becomes less important. The forecast RMSEs from non-assimilative run is considerably larger than those from assimilative run at the first day, but with small changes for increased forecast lead time. At day 3, much smaller difference of the SST RMSE between assimilative and non-assimilative due to the impact of the data from the assimilation is lost over time. The error statistics indicate that the forecast skill from data assimilative run in Monterey Bay is about 2 days. The forcing has an impact at day 3 as compared to persistence where forcing changes are not applied.

Results from data assimilative run and non-assimilative run are compared with independent observations from the R/V Point Sur CTD of MBARI (Haddock et al. 2003) on 20 August 2003 as shown in Fig. 14. Figure 14f displays 7 positions (position 4 and 5 are almost overlapped) for providing observed temperature profiles. The cross sections of temperature in Fig. 14a, b, c are plotted from position 1 to 7. The observations show a shallow thermocline caused by previous upwelling processes, resulting in a very strong vertical gradient of temperature in the
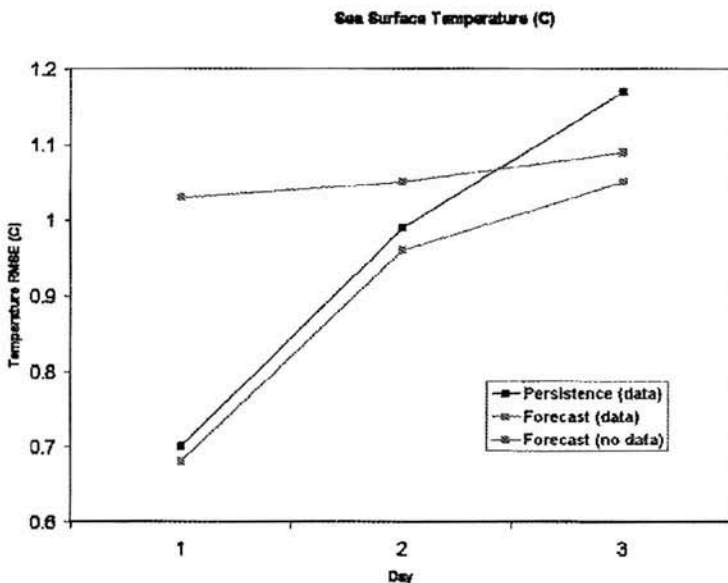

Fig. 13 The domain-averaged persistence and forecast RMSE of SST for August 2003
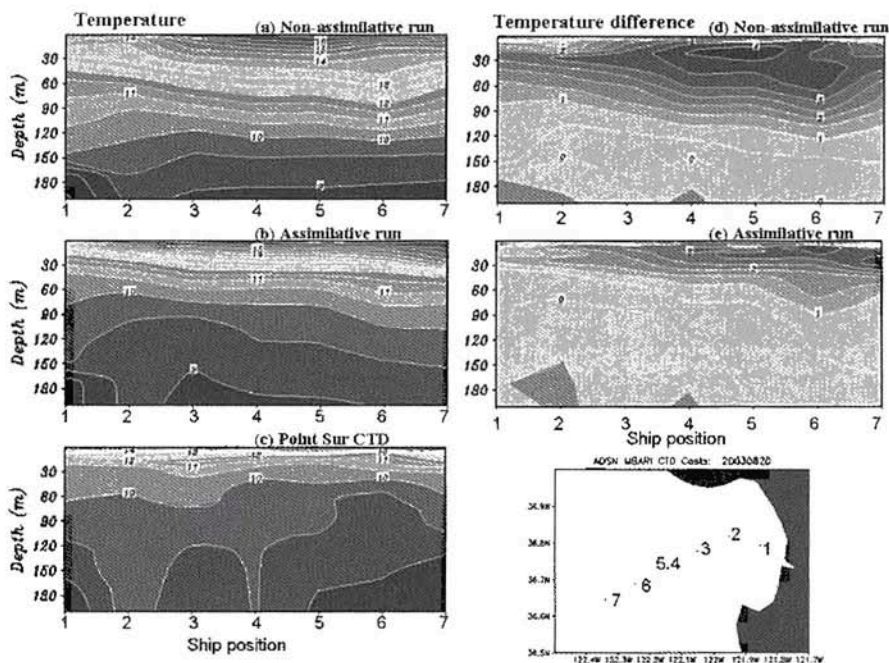
Fig. 14 Cross section of temperature on August 20, 2003 from (**a**) non-assimilative run, (**b**) assimilative run, and (**c**) R/V Point Sur CTD of MBARI. The differences between NCOM forecasts and independent R/V Point Sur CTD observation are shown in (**d**) for non-assimilative run and (**e**) for assimilative rub. The ship positions are shown in (**f**)

upper surface layer (Fig. 14c). Colder water with a temperature of 10°C is located at about 60 m. There is a much smoother thermocline from the non-assimilative run (Fig. 14a), showing a much smaller vertical gradient of temperature in the upper layer. A better thermocline with a larger vertical gradient of temperature closer to the observation is obtained from the assimilative run (Fig. 14b). The temperature contour of 10°C is about 80 and 20 m deeper from non-assimilative and assimilative runs, respectively, indicating warmer temperatures in the upper layers. The temperature differences between the model results and observations reveal a large model bias in the non-assimilative run (Fig. 14d). Both the bias magnitude and its spatial extent are reduced for the model runs with data assimilation (Fig. 14e).

The mean SST biases for the non-assimilative and assimilative runs are dissected for upwelling and relaxation periods to inspect the forecast skills corresponding to different ocean dynamic processes (Fig. 15). The bias of 24 h forecast is averaged for the time period from August 7 to 19 for the upwelling and from August 20 to 24 for the relaxation. The analysis fields from the data assimilative run with all the available data assimilated are used as the "true" state. NCOM model has very good forecast skill for the upwelling center at Point Ano Nuevo, but much less skillful in the south upwelling center (Fig. 15). This leads to a warmer temperature than observation in the south as shown in Fig. 6. Substantial bias during relaxation period (Fig. 15b) denotes that model is less skillful in response to the transition period from
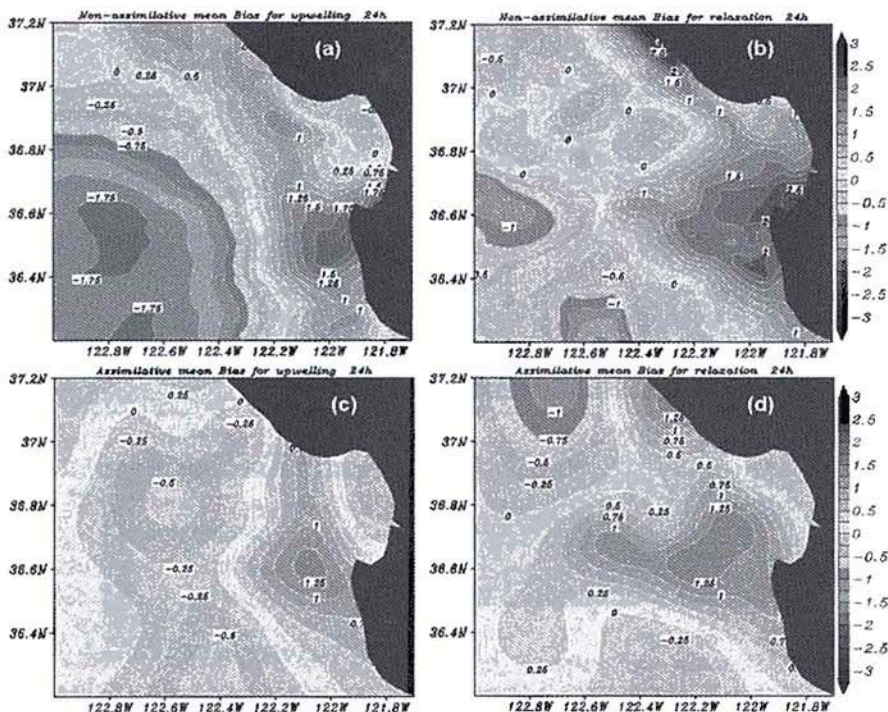
Fig. 15 Mean SST bias of 24 h forecast for non-assimilative run during (**a**) upwelling period and (**b**) relaxation period, and for assimilative run during (**c**) upwelling period and (**d**) relaxation period

upwelling to relaxation wind regime. The errors have larger horizontal scale during the upwelling (Fig. 15a), indicating ocean response to the larger scale wind forcing, and smaller during the relaxation, indicating ocean dynamics dominates the circulation. The biases for both upwelling and relaxation periods are reduced for assimilative run, especially for the relaxation period with the maximum value decreased from 2.75 to 1.25°C. The assimilation of both operational and AOSN II experimental data gives better initial conditions and reduced forecast errors (Fig. 15b, d).

The mean bias errors and RMSE of temperature based on the observation from moorings m1 and m2 for data assimilative run and non-assimilative run during upwelling and relaxation periods for 24, 48, and 72 h forecasts are displayed in Fig. 16. In general, both mean bias and RMSE are smaller for the upwelling and relaxation periods when data assimilation is performed. The difference is more apparent in the seasonal thermocline due to its large variability and uncertainty and the model could misplace it in the simulation. The errors increase with forecast periods, however, they show relatively small error growth. The bias errors from non-assimilative run are smaller than assimilative run in the surface layer during the upwelling period. This could be due to the model response fairly well to the upwelling favorable winds. Similar to the SST bias, there is a lot worse forecast skill during the relaxation period than the upwelling period due to the transition of driving forcing between the wind and ocean dynamics.
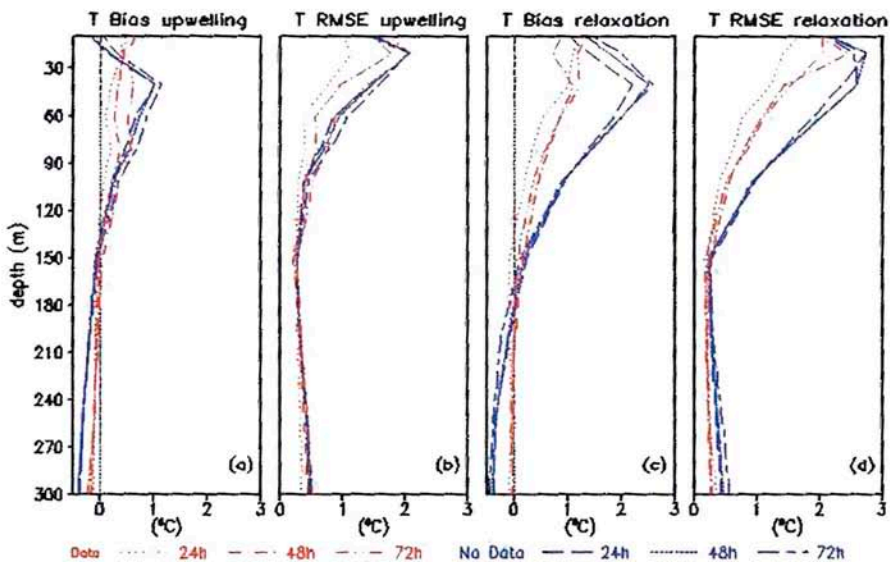
Fig. 16 Mean bias errors and RMSE of temperature based on the observation from moorings m1 and m2 for 24, 48 and 72 h forecasts during upwelling (a and b) and relaxation (c and d) periods. The notation "Data" denotes for data assimilative run and "No Data" for non-assimilative run

7 Summary

This paper presents results from an ocean model (NCOM) and a cycling ocean data assimilation system (NCODA) in the Monterey Bay area in conjunction with the AOSN II field campaign. The multivariate analysis of NCODA is cycled with the ocean forecast model NCOM in a sequential, incremental, update cycle. In addition to operational ocean data from the GODAE server, which include remotely sensed SST and SSH and in situ surface and sub-surface observations of temperature and salinity, the assimilated data included high-density aircraft SST data and high-frequency buoy data from the AOSN II field experiment. The ocean forecast model used hourly atmospheric forcing from COAMPS and 3-hourly lateral boundary conditions from Global NCOM. An assimilative run was set up to cycle NCODA and NCOM for the entire month of August 2003, and results are compared with a non-assimilative NCOM run. The Global NCOM nowcast at 00Z August 1 2003 was used to initialize NCOM for the non-assimilative run and for the first forecast (before data assimilation cycle) of the assimilative run. Statistics for simple persistence, forecast skill, and performance measures of the data assimilation are provided to validate and evaluate the NCOM-NCODA cycling system.

Results from the data assimilative run are compared with the NOAA POES AVHRR SSTs and the temporally-averaged HF radar surface currents. Both of these sets of observations were independent of the model assimilation. The assimilative results are comparable with the observations in capturing the detailed

coastal features such as upwelling and relaxation processes forced by the atmospheric winds during the late summer time period off Point Ano Nuevo and Point Sur in the vicinity of Monterey Bay. There are significant diurnal fluctuations in these processes. During the upwelling period, the upwelled cold water at the surface off Point Ano Nuevo reaches $11.5°C$ with a strong upwelling front positioned between the upwelled and offshore water. The cold water transports through the mouth of Monterey Bay and joins with the cold water upwelled from Point Sur, forming a cyclonic circulation inside the Monterey Bay. During the relaxation period, the upwelled cold water diminishes and is replaced with warm water from offshore with temperature greater than $16°C$ in most of the region. A cyclonic circulation pattern forms inside the bay during the relaxation phase, with an anti-cyclonic circulation outside the bay. These relaxation phase features are well simulated but with a smaller current speed in the inshore cyclone than what is observed.

Diagnosis of the analysis residual with respect to the forecast background error shows that the analysis improves the model initial conditions. The mean innovation RMSE and bias of SST and temperature at depth are reduced from the analysis. The data assimilative forecast is more skillful than the persistence and the non-assimilative run. The data assimilative run is able to simulate a thermocline layer as observed from the R/V Point Sur CTD of MBARI better than the non-assimilative run.

Statistics from forecasts of August 2003 denote that NCOM has more proficient forecast skill during the upwelling period and less skilful during the transition period from upwelling to relaxation wind regime. The biases for both upwelling and relaxation periods are reduced by data assimilation, with a most significant reduction of warm bias from 2.75 to $1.25°C$ for the relaxation period. The most important improvement in forecast due to the data assimilation is reflected for the seasonal thermocline, where large variability and uncertainty exist due to the strong nonlinearity and turbulence.

The results motivate the need to increase the model resolutions in the future in order to improve the forecast skill of the strength of upwelling, upwelling transport and areal extent of upwelling center. An accurate forecast is very important in the data assimilation system so that the assimilated data can be dynamically incorporated into the model trajectory.

Data assimilation with addition data in the coastal area has show very promising results by reducing bias errors and RMSE in both upwelling and relaxation periods, and in the upper seasonal thermocline layer. Other data collected from the AOSN II field campaign, such as glider data and HF radar data are very useful for providing vertical structure and surface current of upwelling and relaxation. We will explore the assimilation of these data sets in our future work.

References

Banta RM, Olivier LD, Levinson DH (1993) Evolution of the Monterey Bay sea-breeze layer as observed by pulsed Doppler lidar. J Atmos Sci 50: 3959–3982

Bishop CH, Toth Z (1999) Ensemble transformation and adaptive observations. J Atmos Sci 56: 1748–1765

Bishop CH, Etherton BJ, Majumdar SJ (2001) Adaptive sampling with the ensemble Kalman Filter, I: Theoretical aspects. Mon Weather Rev 129: 420–436

Chavez F (2003a) M1 Mooring Hydrography and Meteorology Data 2002–2003, Autonomuos Ocean Sampling Network (AOSN) 2003 Field Experiment, Monterey Bay Aquarium Research Institute. Retrieved January 2008 from http://aosn.mbari.org

Chavez F (2003b) M2 Mooring Hydrography and Meteorology Data 2003–2004, Autonomuos Ocean Sampling Network (AOSN) 2003 Field Experiment, Monterey Bay Aquarium Research Institute. Retrieved January 2008 from http://aosn.mbari.org

Chelton DB, deSzoeke RA, Schlax G (1998) Geographical variability of the first baroclinic Rossby radius of deformation. J Phys Oceanogr 28: 433–460

Cummings JA (2005) Operational multivariate ocean data assimilation. Q. J. R. Meteorol Soc 131: 3583–3604

Cummings JA (2006) The NRL real-time ocean data quality control system. NRL Technical Note

Daley R (1991) Atmospheric data analysis. Cambridge University Press, Cambridge, UK

Doyle JD, Jiang Q, Chao Y, Farrara J (2008) High-resolution atmospheric modeling over the Monterey Bay during AOSN II. (To appear Deep Sea Research)

Fox DN, Teague WJ, Barron CN, Carnes MR, Lee CM (2002) The modular ocean data assimilation system. J Atmos Ocean Technol 19:240–252

Haddock SHD, Ryan JP, Herren CM, Brewster J, Orrico CM, and Conlin D (2003) Hydrographic and bioluminescent towfish data from the research vessel Point Sur, Aug. 2003, Autonomuos Ocean Sampling Network (AOSN) 2003 Field Experiment, Monterey Bay Aquarium Research Institute. Retrieved January 2008 from http://aosn.mbari.org

Hodur RM (1997) The Naval Research Laboratory's Coupled Ocean/Atmosphere Mesoscale Prediction System (COAMPS). Mon Wea Rev 125: 1414–1430

Hodur RM, Hong X, Doyle JD, Pullen JD, Cummings J, Martin PJ, Rennick MA (2002) The Coupled Ocean/Atmosphere Mesoscale Prediction System (COAMPS). Oceanography 15(1): 88–89

Hong X, and Bishop CH (2005) COAMPS ocean ensemble forecast system. Presented on the 17th Conference on Numerical Weather Prediction, Washington, DC, 1–5 August 2005. http://ams.confex.com/ams/WAFNWP34BC/techprogram/paper_94771.htm. Accessed 15 December 2007

Hong X, and Bishop CH (2006) COAMPS ocean ensemble forecast and adaptive sampling system. Presented on the 2006 Ocean Sciences Meeting, Honolulu, Hawaii, 20-24 February 2006. http://www.agu.org/meetings/os06/cd/. Accessed 15 December 2007

Hong X, Hodur RM, Martin P (2008) Numerical simulation of deep-water convection in the Gulf of Lion. Pure Appl Geophys 164: 2101–2116

Jerlov NG (1976) Marine optics, Elsevier, 231 pp

Kelly KA (1985) The influence of winds and topography on the sea surface temperature patterns over the northern California slope. J Geophys Res 90: 11783–11798

Kondo J (1975) Air-sea bulk transfer coefficients in diabatic conditions. Boundary-Layer Met 9: 91–112

Martin PJ (2000) Description of the Navy Coastal Ocean Model Version 1.0. Naval Research Laboratory, NRL/FR/7322—00-9962, 1–42

Martin PJ, and Hodur RM (2003) Mean COAMPS air-sea fluxes over the Mediterranean during 1999 report. Naval Research Laboratory, Stennis Space Center, Mississippi

Paduan J, and Lipphardt B (2003) Coastal Ocean Dynamics Applications Radar (CODAR) Data 2003, Autonomuos Ocean Sampling Network (AOSN) 2003 Field Experiment, Monterey Bay Aquarium Research Institute. Retrieved January 2008 from http://aosn.mbari.org

Pickett MH, and Paduan JD (2003) Ekman transport and pumping in the California Current based on the U.S. Navy's high-resolution atmospheric model (COAMPS). J Geophys Res 108 (C10): 3327–3337

Pullen J, Doyle JD, Hodur R, Ogston A, Book JW, Perkins H, and Signell R (2003) Coupled ocean-atmosphere nested modeling of the Adriatic Sea during winter and spring 2001. J Geophys Res v108, C10, 3320,doi:10.1029/2003JC001780

Ramp S (2003) Sea surface remote sensing and atmospheric meteorology from the twin otter aircraft, Aug./Sept. 2003, Autonomuos Ocean Sampling Network (AOSN) 2003 Field Experiment, Monterey Bay Aquarium Research Institute. Retrieved January 2008 from http://aosn.mbari.org

Ramp SR, Paduan JD, Shulman I, Kindle J, Bahr FL, Chavez F (2005) Observation of upwelling and relaxation events in the northern Monterey Bay during August 2000. J Geophys Res v110, C07013, doi: 10.1029/2004JC002538

Rosenfeld LK, Schwing FB, Garfield N, and Tracy DE (1994) Bifurcated flow from an upwelling center: a cold water source for Monterey Bay. Cont Shelf Res 14: 931–964

Shulman I, Kindle J, Martin P, deRada S, Doyle J, Penta B, Anderson S, Chavez F, Paduan J, and Ramp S (2007) Modeling of upwelling/relaxation events with the Navy Coastal Ocean Model. J Geophys Res v112, C06023, doi:10.1029/2006JC003946

Tseng Y.-H. and Breaker LC (2007) Nonhydrostatic simulations of the regional circulation in the Monterey Bay area. J Geophys Res v112, C12017, doi:10.1029/2007JC004093